sustainability

MDPI

Article

Comparative Performance Analysis of a Grid-Connected Photovoltaic Plant in Central Greece after Several Years of Operation Using Neural Networks

Elias Roumpakias and Tassos Stamatelos *

Mechanical Engineering Department, University of Thessaly, 383 34 Volos, Greece
* Correspondence: stam@uth.gr; Tel.: +30-2421-074-067

Abstract: The increasing installed volume of grid-connected PV systems in modern electricity networks induces variability and uncertainty factors which must be addressed from several different viewpoints, including systems' protection and management. This study aims to estimate the actual performance and degradation of photovoltaic (PV) parks in Central Greece after several years of operation. Monitoring data over several years are analyzed and filtered, the performance ratio and normalized efficiency are computed, and five different ANNs are employed: (i) a feed-forward network (one hidden layer); (ii) a deep feed-forward network (two hidden layers); (iii) a recurrent neural network; (iv) a cascade-forward network; and (v) a nonlinear autoregressive network. The following inputs are employed: in-plane irradiance; backsheet panel temperature; airmass; clearness index; and DC voltage of the inverter. Monitoring data from an 8-year operation of a grid-connected PV system are employed for training, testing, and validation of these networks. They act as a baseline, built from the first year, and the computed metrics act as indicators of faults or degradation. Best accuracy is reached with the DFFNN. The ANNs are trained with data from the first year of operation, and output prediction is carried out for the remaining years. Annual electricity generation exceeds 1600 kWh /kWp, and MAPE values show an increasing trend over the years. This fact indicates a possible change in PV performance.

Keywords: photovoltaics; air mass; forecasting; degradation; neural networks

Citation: Roumpakias, E.; Stamatelos, T. Comparative Performance Analysis of a Grid-Connected Photovoltaic Plant in Central Greece after Several Years of Operation Using Neural Networks. *Sustainability* **2023**, *15*, 8326. https://doi.org/10.3390/su15108326

Academic Editor: Jifeng Song

Received: 28 March 2023
Revised: 8 May 2023
Accepted: 18 May 2023
Published: 19 May 2023

1. Introduction

The substitution of renewable energy sources to the electricity grid has been remarkable during the last decade in Europe and elsewhere. European and international legislation for a decrease in greenhouse gas emissions played an important role in this expansion. According to IRENA, at the end of 2021, the capacity of installed global renewable energy reached 3064 GWp. This number comprises about 40% hydropower, 28% solar power, 27% wind power, and 5% other renewable power sources [1]. Renewable electricity production capacity has also shown a significant increase in Greece, where 41.48% of total electricity was generated from renewable energy sources (RES) in 2021 [2]. A remarkable number of fossil-fuel power-generation plants have been phased out from the Greek system. This has resulted in excessive electricity prices in the market as it coincided with significant increases in international natural gas prices in 2022, causing a new energy crisis that is yet to be contained. This situation creates challenges for further renewable energy investments, especially in photovoltaic (PV) systems.

1.1. Photovoltaic Systems Applications

An intense interest for investment is observed in this area by citizens, companies, energy communities, and the public sector. There are different modes of photovoltaic application contracts in Greece. Net metering, virtual net metering for energy communities, feed-in tariffs, and feed-in premiums are the main modes for grid-connected systems in both plants and buildings with a typical lifespan of 20–25 years. PV systems mainly support distributed energy generation to achieve effective integration into grids and micro-grids. There are a large number of studies one could cite as examples, which address the combination of ground-coupled heat pumps for upgraded post-COVID-19 ventilation systems [3], rooftop PV combination with hybrid condensing radiant tubes' heating systems [4], and incorporation into residential buildings with air-to-water heat pump systems [5]. Accelerated vehicle electrification is pushing for further expansion of PV systems. This includes smart office buildings' energy systems with rooftop PV systems exploiting electric vehicle battery storage [6], innovative building blocks in Germany with combined heat and power (CHP), battery storage and exploitation of electric vehicles storage [7], and modular packages of electric vehicle charging stations in China, designed to charge 1000 electric vehicles using PV and battery energy storage systems [8]. PV systems in combination with large-capacity battery systems is another important application area [9]. Here, an efficient energy management system that handles on-site PV production with battery energy storage minimizes power exchange with the grid. Interest in classic investments in PV parks is significant and exploits double utilization of land with agrivoltaics, which utilize the land around the PV panels for food-producing crops [10]. Jamil et al. studied the potential of agrivoltaics in Canada using bifacial PV for single-axis tracking and vertical system configurations [11]. The combination of photovoltaic systems with hydrogen systems is gaining increased popularity in research. Important technical parameters of an integrated PV–hydrogen system include the PV tracking system coefficient, PV conversion efficiency, electrolyzer efficiency, and electrolyzer degradation coefficient [12]. Other studies have analyzed a PV-based fuel-cell power system [13], a CES (composite energy station) combined with a PV power-generation system, fuel cell, hydrogen production, hydrogen storage, hydrogenation, and charging, in order to supply energy for electric vehicles (EVs) and hydrogen fuel-cell vehicles (HFCVs) [14].

Now, the uncertainty in predicting solar radiation is a major issue affecting the successful forecasting PV power output, which is essential to sizing, control system optimization, and economic analysis of the above-mentioned systems. Exploitation of data from grid-connected photovoltaic systems is a valid approach that provides significant information regarding this problem. Furthermore, performance analysis of grid-connected PV systems supports PV power forecasting. Economic evaluation of this type of project depends on a good understanding and modeling of degradation of photovoltaic systems that should rely on actual performance data. In the real world environment, all kinds of modules exhibit lower efficiency compared to the manufacturers' specifications [15]. Performance analysis gives a clear view of systems' performance under real life conditions. Thus, it is an important task to be tackled with scientifically sound approaches with an important impact on both the design and evaluation stages of new and existing plants.

1.2. Photovoltaic Performance Analysis Approaches

Performance analysis is based on mathematical models, linear regression models, and the use of specialized software and is widely supported by the use of neural networks.

Neural networks (NNs) have proven invaluable to the performance analysis of renewable energy sources, especially photovoltaics and power forecasting of generation and consumption. All the applications differ in various aspects, e.g., input data, data preprocessing, ANN type and structure, parameter configuration, hybrid application, and performance [16]. The primary neural network types utilized for power forecasting include multi-layer perceptron (MLP), the feed-forward deep neural network (DNN [17]), long short-term memory networks (LSTMs), and convolutional neural networks (CNNs) [17]. Power-generation forecasting studies of PV systems use different types of NNs, with a selection from several inputs and outputs. A distinction of the various approaches is based on the type and standardization of available data. López Gómez et al. combined data from a numerical weather prediction model with an artificial neural network (ANN) model in order to forecast power generation from a PV system using actual temperature and solar irradiation data [18]. Gopi et al. developed a PV system annual yield and performance ratio (PR) forecasting model based on three environmental input parameters: solar irradiance, wind speed, and ambient air temperature. They employed data from a 2 MWp grid-connected PV system and three different machine-learning techniques: an adaptive neuro-fuzzy inference system (ANFIS); response surface methodology (RSM), which is a combination of statistical and mathematical approaches and allows one to determine the independent variable that, when changed, results in the responsible variable having an optimal value; and an ANN [19]. Kolsi et al. compared various artificial intelligence (AI) models based on daily data and seven seasonal models were employed to predict solar potential: simple average (SA); simple moving average (SMA), nonlinear autoregressive (NAR); support vector machine (SVM); Gaussian process regression (GPR); and NN. The results were evaluated based on the root mean square error (RMSE) and mean absolute percentage error (MAPE [20]). Lim et al. proposed a hybrid CNN–LSTM model. The CNN classifies weather conditions, while the LSTM is trained to classify power-generation characteristics. Typical results produce an MAPE of 4.58% on a sunny day and 7.06% on a cloudy day [21]. Suresh et al. proposed a convolutional neural network (CNN) approach consisting of different architectures, namely multi-headed CNN and CNN–LSTM based on data preprocessing techniques to make accurate forecasts using irradiance, module temperature, ambient temperature, and wind speed for short-term forecasting [22]. Andrade et al. used an MLP, RNN, and LSTM to forecast photovoltaic energy from data collected from the PV system in Brazil. The MLP performed adequately, requiring less training time [23]. Kim et al. proposed a combination of a two-step NN bi-directional long short-term memory (BD-LSTM) model with an ANN model using exponential moving average (EMA) preprocessing of historical hourly input data of horizontal radiation, ambient temperature, and surface temperature [24]. Preda et al. proposed an SVM, and data were collected from a cheap data logger and from an API weather station with good prediction results in the estimation of the PV generated power, supporting micro-grid operation [25]. Meltek et al. proposed a model to predict the effect of the panel electric power of a photovoltaic thermal (PV-T) system using LSTM and MLF. Mean absolute error (MAE), RMSE, MAPE, and R^2 correlation coefficients were used as performance metrics [26].

Another important aspect of performance analysis is fault detection using neural networks, IR-thermography electroluminescence images, or a combination thereof. Neural network fault diagnosis of PV systems is generally based on historical data, relevant data related to voltage, current, power, and I–V curves. Images are also employed as inputs [27]. Samara et al. proposed a fault-diagnosis algorithm based on a nonlinear autoregressive exogenous (NARX) neural network that can detect multiple faults, such as open and short-circuit degradation, faulty maximum power point tracking (MPPT), and conditions of partial shading [28]. Onim et al. proposed a CNN to detect dust accumulation on PV panels using a dataset of images of dusty and clean panels. The results demonstrated high accuracy levels [29]. Selvaraj et al. proposed a method for accurate diagnosis of environmental faults using CNN and thermal images for classification of these faults [30]. Lu et al. proposed a fault-diagnosis method to diagnose different PV faults using a proposed dual-channel CNN, which automatically extracts features and weights them to diagnose partial shading conditions and open-circuit faults [31]. Yu et al. proposed dimension-reduction technology mapping multiple-sequence signals to a sequence of images processed by a CNN. Validation carried out on self-made solar power stations proved to be effective in identifying key operation conditions from historical data with negligible loss of features at the presence of mismatched phenomena [32]. Dust accumulation is an important factor; thus, many researchers use neural networks in order to study this effect [33,34].

Except from ANNs, performance analysis procedures are based on statistical or other performance metrics. Most of these approaches are based on comparative analysis. Iqbal et al. proposed a fault-detection method based on string level comparison of DC power of actual and simulated PV plants with the aid of a statistical tool based on Student's t-test [35]. Minai et al. analyzed performance data of a 467.2 kWp grid-connected PV system using array, inverter and system efficiency, performance ratio (PR), and capacity utilization factor (CUF). These parameters are evaluated and compared with similar systems in different regions of the world [36]. Karahüseyin et al. analyzed the performance of a mid-scale crystalline silicon (c-Si) PV system with different orientations and tilt angles in the same region for four years of outdoor exposure, using statistical methods to calculate PLRs; seasonal and trend decomposition using locally weighted scatterplot smoothing (STL); classical seasonal decomposition; and year-on-year methods coupled with PR, temperature-corrected PR, and weather-corrected PR [37]. Agyekum et al. used the PR, degradation, energy-loss prediction, and the PVsyst simulation model to study the performance of solar photovoltaic (PV) modules under Russian weather conditions [38]. Shin et al. proposed a weather-corrected index, linear regression method, temperature-correction equation, estimation error matrix, clearness index and proposed variable index, a one-class support vector machine (SVM) method, and a kernel technique to classify the fault state and anomaly output power of PV plants [39]. Phuong Truong et al. presented a method to estimate the yield and analyze the performance of a grid-connected PV system in a MATLAB/Simulink environment for a rooftop PV system and a solar farm [40]. Dhimish et al. presented degradation rates over a 10-year span for seven different PV systems located in England, Scotland, and Ireland using a power-irradiance technique that compares output measured power with a corresponding irradiance level [41]. Bansal et al. conducted a long-term performance and degradation study based on IEC standard 61724 guidelines from actual data (incident solar irradiation, ambient and module temperature and generated electricity) with annual linear degradation rates found in the range of 0.9 to 1.1% for normal field modules with no visible degradation and 0.97 to 2.9% for visually degraded modules. Mean and median values were 1.8% and 1.6%, respectively, within a six-year operational period [42].

Despite the significant progress in the performance analysis of PV systems, there exists ample room for further improvements. It is important to deploy data from grid-connected PV systems to support the creation of tools that either predict the energy generation of PV systems or evaluate their performance. Nowadays, PV systems are equipped with advanced monitoring systems that can collect a variety of useful performance data. There exist specific studies that propose methods to collect and systematically process these data, as in [43] where a procedure for the automatic transfer of recorded data is described.

In the present paper, actual data collected from grid-connected photovoltaic systems in Central Greece are studied by means of several ANN types and statistical analysis. The objectives of this paper concern the performance evaluation of grid-connected PV systems after several years of operation, assisted by five different ANN types. The novelty of this approach lies in the deployment of actual data for 8 years of operation and the careful selection of inputs for ANN training, taking into account the quality of the atmosphere by use of clearness index and air mass.

The structure of this paper is as follows. Section 2 presents the methodology, consisting of three base steps: (i) statistical and efficiency observations of available data; (ii) data preprocessing; (iii) statistical and efficiency metrics calculations; and (iv) use of five NNs with five inputs. Section 3 presents the solar potential of Central Greece, observations of important performance metrics, comparative analysis among the five ANNs, and investigation into the PV systems' degradation during the 8-year period. The results are analyzed and discussed. Conclusions and proposals for future work are presented in Section 4.

2. Materials and Methods

The proposed methodology exploits actual data from grid-connected photovoltaic systems in Central Greece. A grid-connected 99.84 kWp PV park in Central Greece was monitored. The PV park comprised 416 PV panels on the park, mounted in a fixed south-facing position at a 25 degree tilt angle. A total of 8 inverters were employed in the DC/AC transformation, with technical characteristics presented in Appendix A. The following parameters were monitored in 15 min intervals: solar irradiance; back panel temperature; ambient temperature; DC voltage to the inverter; and AC power output from the inverter. The data employed in the specific work refer to the period from 2013 to 2020. The system's technical data and monitoring and measurement equipment are summarized in Appendix A.

2.1. Statistical and Efficiency Observations of Available Data

The first step of the methodology is to observe the dependence of performance on parameters such as irradiance, clearness index, temperature, and air mass. The main meteorological factors affect the solar power forecast in the following descending order: solar radiation; sunlight; wind speed; temperature; cloud cover; and humidity [44]. Ambient temperature, solar irradiance, and wind speed as meteorological impact factors of PV module temperature are affected by each other [45].

2.2. Data Preprocessing

The second step is a preprocessing methodology that acts as a quality-assurance procedure to the available dataset in order to remove outliers. Data preprocessing in important because of stationary and non-stationary components in the input data that are variable and unpredictable due to weather conditions [46]. The accuracy of the forecasting results is enhanced when preprocessed input data are used [47]. Specific criteria are defined for cleaning up the data, with regard to irradiance, air mass, and inverter power output. Recordings with zero values of inverter power output are rejected and the same is carried out for those with irradiance values <20 W/m^2. Air mass is an important indicator taken into account during data preprocessing. According to previous experience, data records with AM > 10 are not taken into account.

2.3. Statistical and Efficiency Metrics Calculations

Following preprocessing, performance evaluation metrics were calculated as performance ratio calculation (IEC 61724) [48] and normalized efficiency to STC conditions as described in [49]. It is important to compute energy baseline generation; thus, the application of five neural networks was applied using data from the first year of operation. Data from other years are typically applied in neural networks in order to observe deviation from actual data. Trained networks include FFANN, DFFNN, RNN, CFFNN, and NARX. There are five inputs for training and simulation, namely plane irradiance, backsheet panel temperature, air mass, clearness index, and DC voltage of the inverter. It is important to introduce information for atmospheric parameters with air mass and clearness index. Solar spectrum is affected by atmospheric parameters and cloud conditions, which result in estimation error, and it is necessary to consider the solar spectrum change in highly accurate PV output forecasting [50].

2.4. Feed-Forward Neural Network (Network1)

One of the most well-known artificial neural networks is a perceptron. It is composed of an input layer, a hidden layer, and an output layer (see Figure 1, hyper-parameters in Table 1). The neurons in the layers are linked by synaptic weights. These weights can be determined with the use of the learning process [51]. There are five inputs for training and simulation, namely plane irradiance, backsheet panel temperature, air mass, clearness index, and DC voltage of the inverter. Neural networks consist of one hidden layer with twenty nodes and one output layer. The Levenberg–Marquardt optimization algorithm is employed for training.

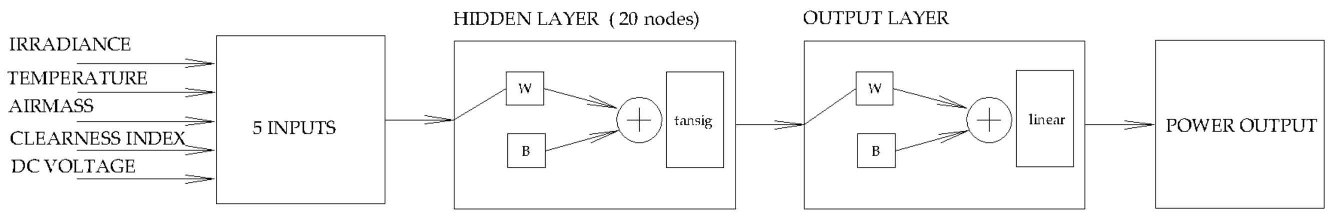

Figure 1. Feed-forward neural network architecture.

Table 1. Design parameters of the specific type of FF ANN applied, along with the hyper-parameter values related to the training procedure.

ANN Type	FFANN
ANN dimensions	
Inputs	5
Layers	2
Outputs	1
Input delays	0
Layer delays	0
Weight elements	141
ANN connections	
Bias connections	[1; 1]
Input connections	[1; 0]
Layers connections	[0 0; 1 0]
Output connections	[0 1]
ANN training hyper-parameters	
Maximum epochs	1000
Maximum training time	Inf
Performance goal	0
Minimum gradient	1.00×10^{-7}
Maximum validation checks	**10**
μ_k	0.01
μ_k decrease ratio	0.1
μ_k increase ratio	10
Maximum μ_k	1.00×10^{10}

2.5. Deep Feed-Forward Neural Network (Network2)

Deep FF ANNs (DFFNNs) are neural networks consisting of more than three layers (input layer, many hidden layers, and output layer) [52]. A neural network with at least two layers qualifies as a deep neural network [53]. Inputs for training and simulation include in-plane irradiance, backsheet panel temperature, airmass, clearness index, and DC voltage of the inverter. Neural networks consist of two hidden layers with twenty nodes and one output layer (see Figure 2, hyper-parameters in Table 2). The Levenberg–Marquardt optimization algorithm is employed for training.

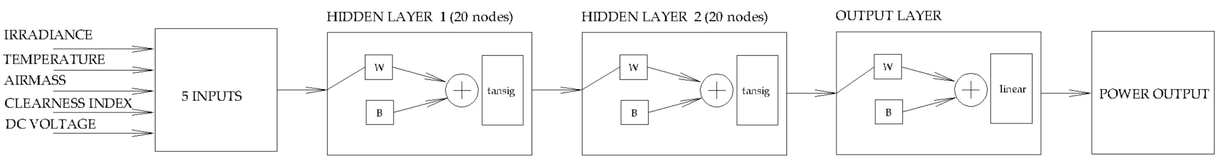

Figure 2. Deep feed-forward neural network architecture.

2.6. Recurrent Neural Network (Network3)

RNNs are an extension of conventional FFNNs, i.e., feedback, which are able to use the last-time step output as the input at each node [54]. Inputs for training and simulation include in-plane irradiance, backsheet panel temperature, airmass, clearness index, and DC voltage of the inverter. Neural networks consist of two hidden layers with twenty nodes and one output layer (see Figure 3, hyper-parameters in Table 3). The Levenberg–Marquardt optimization algorithm is employed for training.

Table 2. Design parameters of the specific type of DFFNN applied, along with the hyper-parameter values related to the training procedure.

ANN Type	DFFNN
ANN dimensions	
Inputs	5
Layers	3
Outputs	1
Input delays	0
Layer delays	0
Weight elements	561
ANN connections	
Bias connections	[1; 1;1]
Input connections	[1; 0;0]
Layers connections	[0 0 0; 1 0 0;0 1 0]
Output connections	[0 0 1]
ANN training hyper-parameters	
Maximum epochs	1000
Maximum training time	Inf
Performance goal	0
Minimum gradient	1.00×10^{-7}
Maximum validation checks	10
μ_k	0.001
μ_k decrease ratio	0.01
μ_k increase ratio	10
Maximum μ_k	1.00×10^{10}

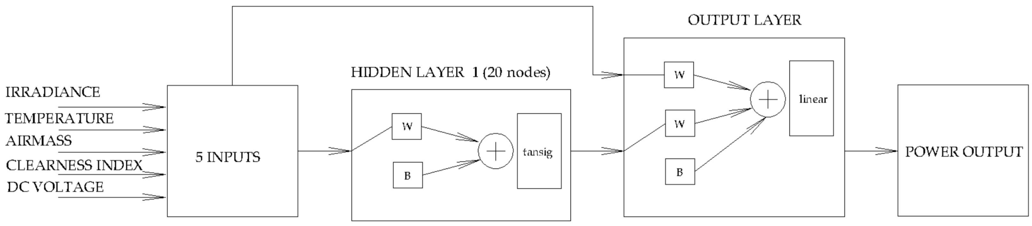

Figure 3. Recurrent neural network architecture.

2.7. Cascade-forward Autoregression Model (Network4)

Cascade-forward neural networks (CFNNs) also consist of input, hidden, and output layers in which neurons are arranged. In terms of operation, CFNNs are comparable to FFNNs [55]. Inputs for training and simulation include in-plane irradiance, backsheet panel temperature, airmass, clearness index, and DC voltage of the inverter. Neural networks consist of two hidden layers with twenty nodes and one output layer (see Figure 4, hyper-parameters in Table 4). The Levenberg–Marquardt optimization algorithm is employed for training.

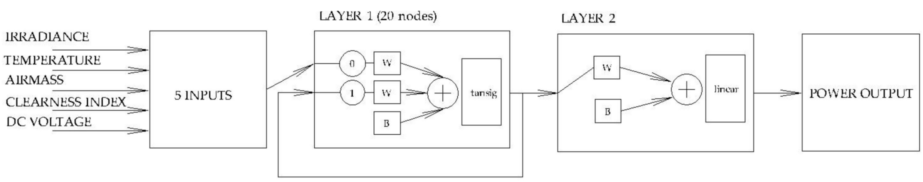

Figure 4. Cascade-forward neural network architecture.

Table 3. Design parameters of the specific type of RNN applied, along with the hyper-parameter values related to the training procedure.

ANN Type	**RNN**
ANN dimensions	
Inputs	5
Layers	2
Outputs	1
Input delays	0
Layer delays	0
Weight elements	146
ANN connections	
Bias connections	[1; 1]
Input connections	[1; 0]
Layers connections	[0 0; 1 0]
Output connections	[0 1]
ANN training hyper-parameters	
Maximum epochs	1000
Maximum training time	Inf
Performance goal	0
Minimum gradient	1.00×10^{-7}
Maximum validation checks	6
μ_k	0.001
μ_k decrease ratio	0.1
μ_k increase ratio	10
Maximum μ_k	1.00×10^{10}

Table 4. Design parameters of the specific type of cascade-forward neural network applied, along with the hyper-parameter values related to the training procedure.

ANN Type	**CFNN**
ANN dimensions	
Inputs	5
Layers	2
Outputs	1
Input delays	0
Layer delays	1
Feedback delays	1
Weight elements	541
ANN connections	
Bias connections	[1; 1]
Input connections	[1; 0]
Layers connections	[0 0; 1 0]
Output connections	[0 1]
ANN training hyper-parameters	
Maximum epochs	1000
Maximum training Time	Inf
Performance goal	0
Minimum gradient	1.00×10^{-7}
Maximum validation checks	10
μ_k	0.001
μ_k decrease ratio	0.01
μ_k increase ratio	10
Maximum μ_k	1.00×10^{10}

2.8. Non Linear Autoregression Exogenous (Network5)

NARX is a recurrent dynamic neural network, has feedback connections which enclose several layers of the network for nonlinear time series prediction [56]. NARX is a partial recurrent neural network (RNN) as its memory is embedded into the network [57]. Five inputs for training and simulation are employed: in-plane irradiance, backsheet panel temperature, airmass, clearness index and DC voltage of the inverter. Neural networks consist of two hidden layers with twenty nodes and one output layer (see Figure 5, hyper-parameters in Table 5). The Levenberg–Marquardt optimization algorithm is employed for training.

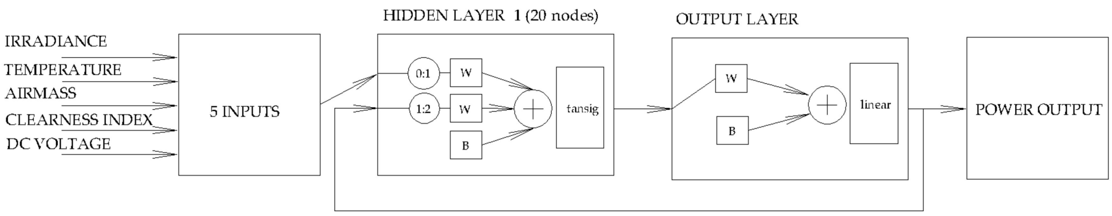

Figure 5. Nonlinear autoregression exogenous neural network architecture.

Table 5. Design parameters of the specific type of NARX neural network applied, along with the hyper-parameter values related to the training procedure.

ANN Type	**NARX**
ANN dimensions	
Inputs	5
Layers	2
Outputs	1
Input delays	1
Layer delays	2
Feedback delays	2
Weight elements	281
Sample time	1
ANN connections	
Bias connections	[1; 1]
Input connections	[1; 0]
Layers connections	[0 0; 1 0]
Output connections	[0 1]
ANN training hyper-parameters	
Maximum epochs	1000
Maximum training Time	Inf
Performance goal	0
Minimum gradient	1.00×10^{-7}
Maximum validation checks	6
μ_k	0.001
μ_k decrease ratio	0.1
μ_k increase ratio	10
Maximum μ_k	1.00×10^{10}

The performance analysis methodology involves the application of the first years' (2013) data in training with the above types of neural network. Five input parameters are employed: in-plane irradiance; backsheet panel temperature; air mass; clearness index; and DC voltage of the inverter.

3. Results and Discussion

This section is divided in terms of statistical results of energy generation in correlation with environment conditions and results from the application of neural network simulation.

3.1. Statistical and Efficiency Metrics

3.1.1. Energy Generation in Correlation with Environment Conditions

As discussed in Section 2, the correlation of energy production with weather and atmospheric parameters is important in order to evaluate data. Figure 6 shows that more than 90% of electricity is generated for air mass values <3. In terms of irradiance (Figure 7), only 7.5% of electricity is produced at low irradiance levels. Consequently, rejection of values with irradiance <20 W/m^2, which represents 0.1% of energy generation, was adopted.

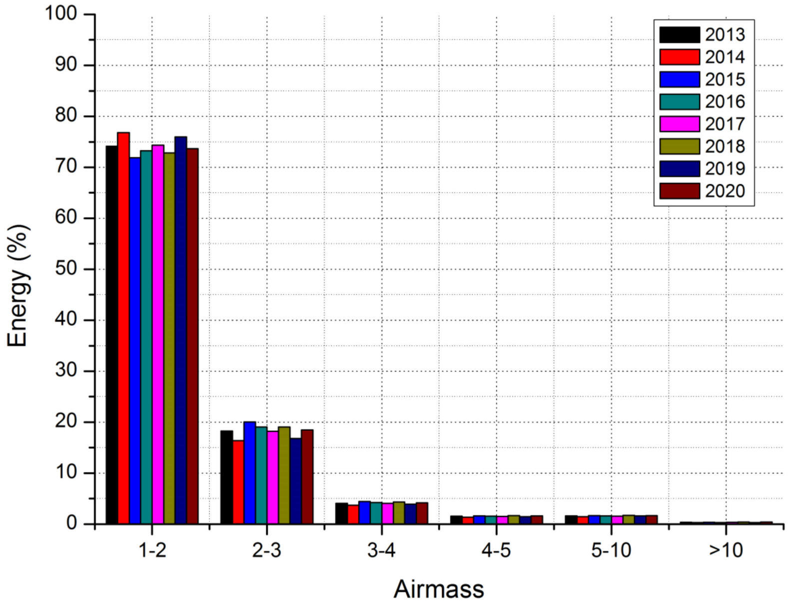

Figure 6. Electricity generation distribution among the various air mass classes.

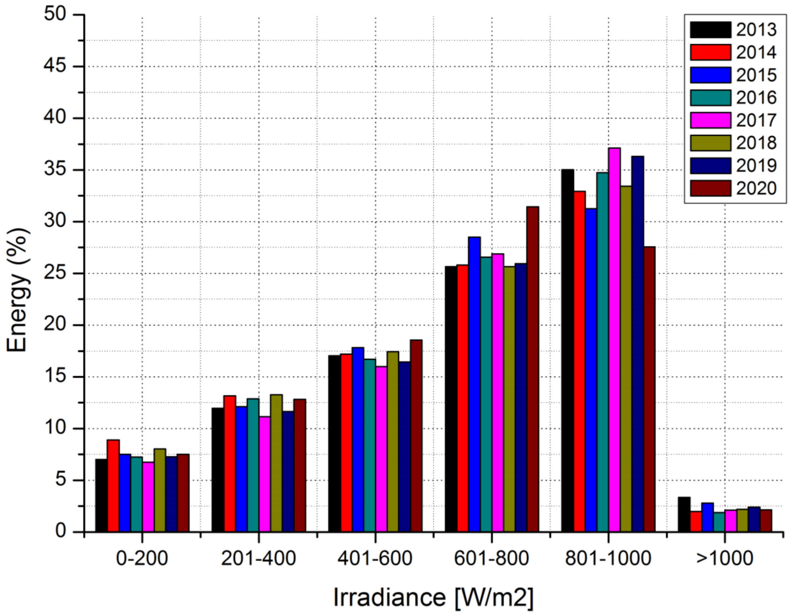

Figure 7. Electricity generation distribution among the various irradiance classes.

Temperature has a negative impact on the energy generation of PV systems. Figure 8 shows that 65% of energy is generated when the temperature is higher from 35 °C.

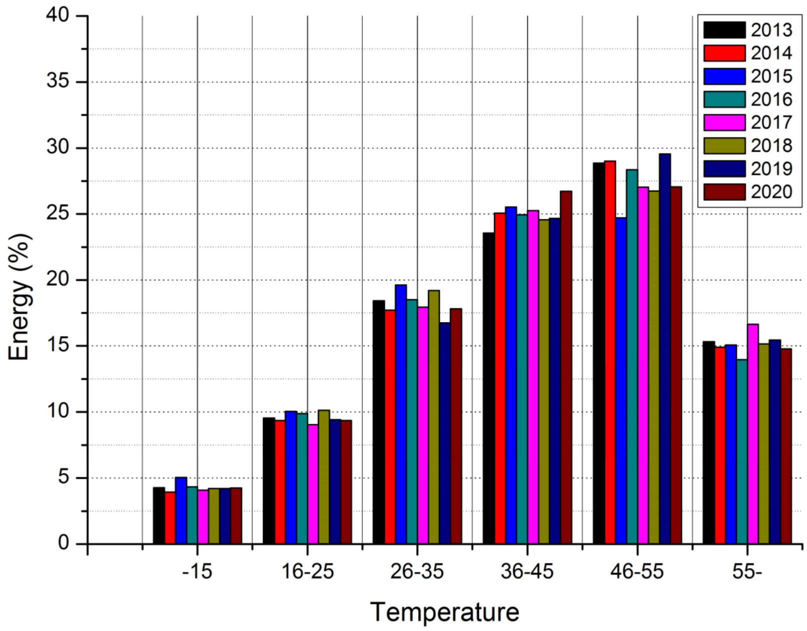

Figure 8. Electricity generation distribution among the various temperature classes.

3.1.2. Efficiency Metrics

Energy generation from one inverter of nominal power 12.84 kWp fluctuated between 17,986 and 20,111 kWh per year. Furthermore, energy generation per installed DC power fluctuated between 1437.1 and 1611.5 kWh/ kWp (see Table 6). The maximum generation was observed during the first year of operation. The analysis procedure was based on comparison of efficiency metrics of each year with that of the first year.

Table 6. Energy generation from 8-year period.

Year	2013	2014	2015	2016	2017	2018	2019	2020
kWh	20,111	17,986	19,069	19,049	19,498	17,935	18,600	18,816
kWh/kWp	1611.5	1441.2	1528.0	1526.4	1562.4	1437.1	1490.4	1507.7

As observed in Figure 6, the most significant air mass classes are those from 1 to 3. In these classes, efficiency fluctuated between 12.84–13.86% and 13.07–14.73%, respectively, according to Table 7. Maximum values were reported during the first year of operation and lower values were reported during 2019.

Table 7. Averaged efficiency in several air mass classes during 8-year period.

	Efficiency							
	%	%	%	%	%	%	%	%
AM	2013	2014	2015	2016	2017	2018	2019	2020
1–2	13.86	13.80	13.72	13.25	13.39	13.25	12.84	13.45
2–3	14.73	14.44	14.39	13.99	13.91	13.99	13.07	14.11
3–4	14.85	14.35	14.59	13.99	14.21	14.04	13.36	14.04
4–5	14.58	14.09	14.00	13.74	13.80	13.66	13.32	13.80
5–10	13.54	13.41	12.96	12.84	13.05	12.94	12.65	13.00
>10	11.74	11.81	11.02	11.04	11.19	11.17	11.02	11.07

In order to decouple the effect of temperature, a normalized efficiency was calculated (Section 2), which is presented in Table 8. In the first two classes, normalized efficiency fluctuated between 13.98 to 15.08% and 13.21% to 14.87%, respectively. Maximum values were reported during the first year of operation and the lowest values were reported during

2019. It was observed that during 2014, electricity generation values were minimized. However, efficiency and normalized efficiency values were the maximum values observed after the first year of operation. This is indicative of the importance of weather conditions in electricity generation. The stochastic nature of insolation is one of the main problems in evaluating PV systems' performance and energy forecasting.

Table 8. Averaged normalized efficiency in several air mass classes during 8-year period.

	Normalized Efficiency							
	%	%	%	%	%	%	%	%
AM	2013	2014	2015	2016	2017	2018	2019	2020
1–2	15.08	14.91	14.81	14.39	14.59	14.34	13.98	14.62
2–3	14.87	14.50	14.57	14.10	14.07	14.10	13.21	14.28
3–4	14.67	14.14	14.40	13.80	14.04	13.85	13.22	13.87
4–5	14.28	13.77	13.67	13.44	13.51	13.37	13.06	13.50
5–10	13.12	12.99	12.54	12.44	12.65	12.55	12.29	12.60
>10	11.19	11.26	10.51	10.53	10.68	10.64	10.52	10.53

Another important metric for system evaluation is performance ratio. However, this metric cannot take into account the temperature effect. Figure 9 presents the evolution of the daily PR for this period, which was observed to fluctuate from 0.8 to 0.96. The effect of temperature is clearly depicted in Figure 9, where the PR had a decreasing trend in the summer months (due to the higher temperature values). Taking into account Figure 8, where it is observed that an important part of energy generation is produced when the temperature is higher than 35 °C, it seems that PR and efficiency alone cannot provide clear results. It is important to take into account additional factors during days with specific, already known faults. Such faults concern problems with the grid, electrical faults, faults in string fuses, days with snow cover, and problems with sensors in the monitoring system.

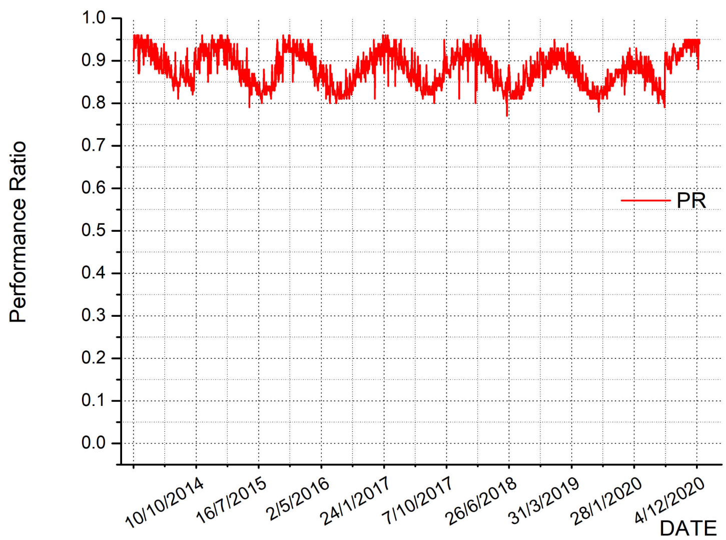

Figure 9. Performance ratio variation during the 8-year period.

Figures 10–13 present the measured power and irradiance in correlation with the daily PR and the Kt daily clearness index. Figure 10 shows observations from spring days when the clearness index varied from 0.29 to 0.7. These limits differentiate a clear-sky day from a cloudy day for this period of the year. The performance ratio was observed to fluctuate in a narrow range from 0.91 to 0.96, indicating the absense of faults.

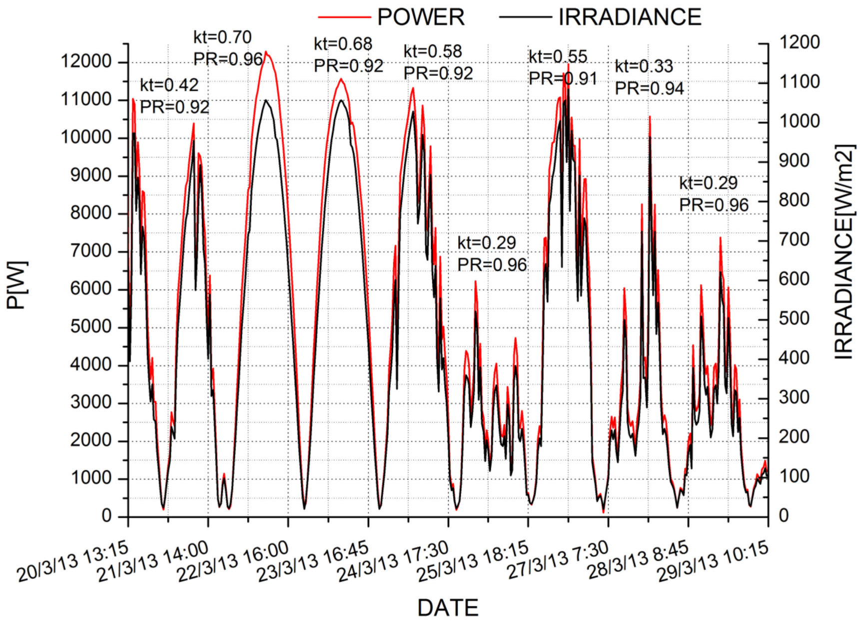

Figure 10. Cloudy and sunny days during March of 2013.

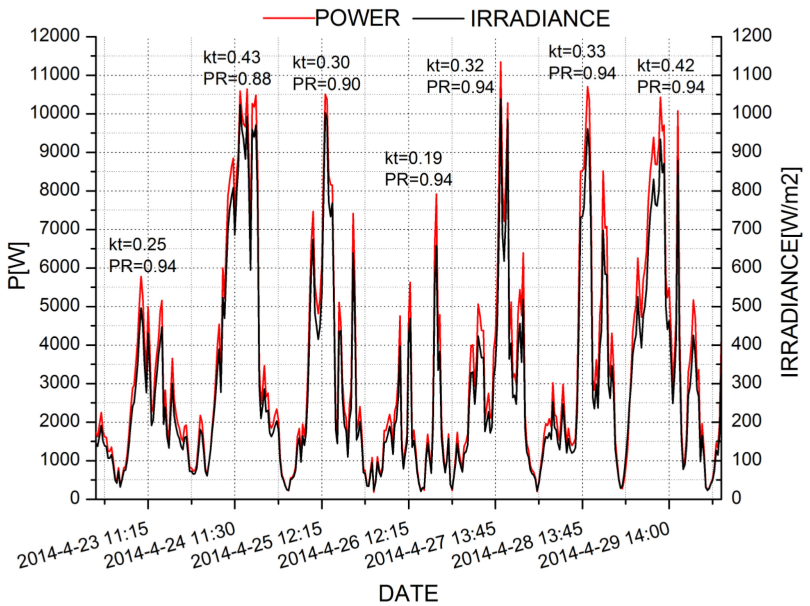

Figure 11. Several cloudy days during April 2014.

During cloudy days, the clearness index fluctuated significantly, as depicted in Figure 11. There were days with significant irradiance fluctuations. For example, irradiance levels were high in the example of 29 April 2014 when the clearness index was 0.42 and the PR was 0.94. On the other hand, during totally cloud covered days, values of the clearness index at 0.19 to 0.25 were reported.

Comparing clear-sky days during summer (Figure 12) and clear-sky days during spring (Figure 10), it was observed that values of clearness index fluctuate from 0.5 to 0.7. Furthermore, PR values are lower during clear-sky summer days compared to the spring's clear-sky days.

Clearness index values were reported below 0.1 during totally cloudy days of winter. On the other hand, values between 0.5–0.65 were observed during clear-sky days. Clearness index values varied from 0.5 to 0.7 for clear-sky days depending on the month.

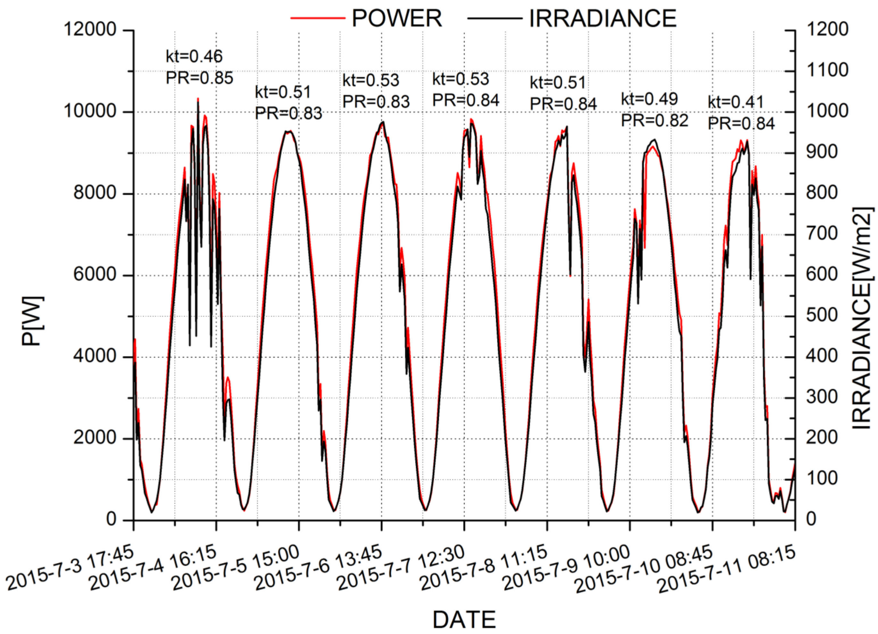

Figure 12. Summer days during July of 2015.

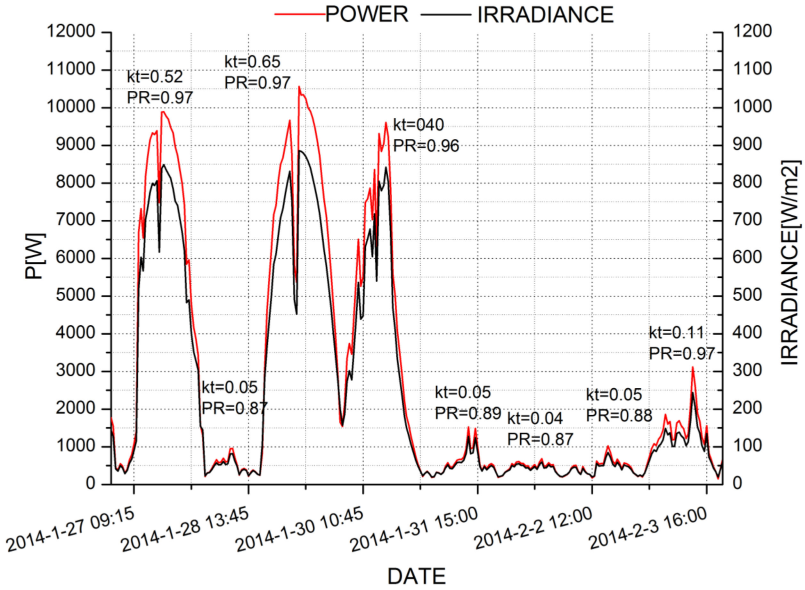

Figure 13. Winter days during winter January–February of 2015.

3.2. Neural Networks Simulation

The proposed methodology is based on the comparative analysis of the application of neural networks on the available data. First, it is important to observe the NN behavior. To this end, the predictions of five types of NN were compared with real values for spring clear-sky days of 2014. Figure 14 shows this comparison for 10 April 2015 to 13 April 2015 when clearness index values were 0.59 to 0.65 and PR values were 0.88 to 0.91, respectively. A general trend in these clear-sky days is that the MAPE varied from 1.90% (DFANN) to 3.42% (NARX). Taking account of the MBE metric positive values (Table 9), it is clear that all networks overestimated power. FFANNs and DFFNNs have lower fluctuations on performance metrics.

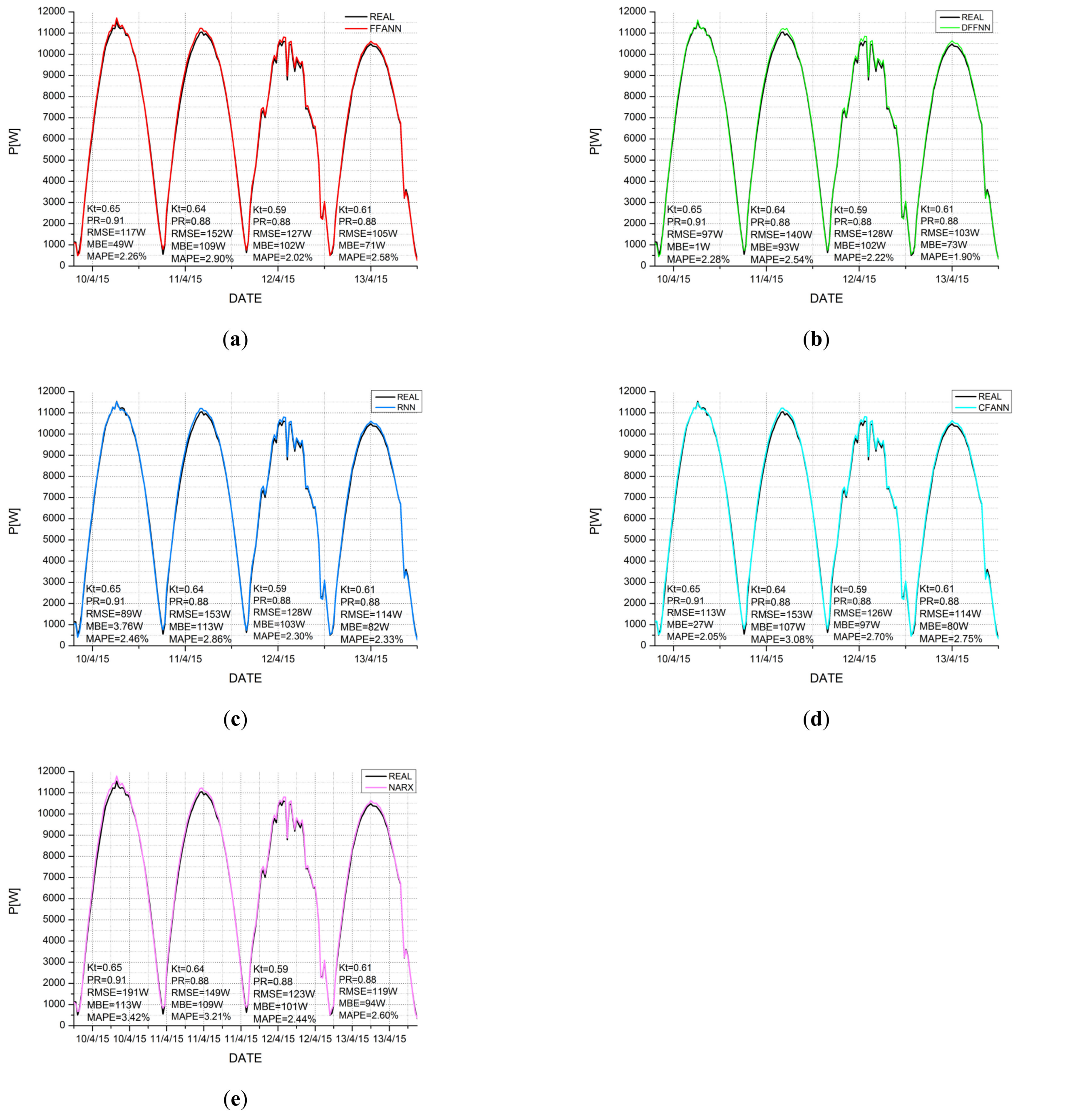

Figure 14. Predicted and real values of power during clear-sky days of (**a**) FFNN; (**b**) DFNN; (**c**) RNN; (**d**) CFN; and (**e**) NARX.

The goal of the proposed methodology is the long-term performance analysis based on comparing simulated values with real values of power. The proposed neural network types were trained with data from the first year of operation, which acted as the baseline operation. Deviation from baseline values is an indicator of possible faults, degradation problems, and dust accumulation effects. This section investigates which of the proposed models is better for baseline.

Furthermore, it is important to evaluate the NN performance for different years. Figure 15 shows the fluctuation in daily MAPE for five NNs during the year 2014, which was the first year of evaluation. A box plot (Figure 15) for 2014 shows that the error for DFFNN and FFANN is lower than the error of the other networks, and the median values are reported around 3.7%. The MAPE of NARX is reported to be of a higher value during

2014, especially the median values of around 4.2%, with the next higher values reported for RNN with median values of around 4.2%. CFN shows slightly higher values than DFFNN and FFANN with median values of around 3.9%. Figure 15 shows that the MAPE values for the year of 2014 are reported to be between 3.7% and 4.2%, depending on the type of neural network. The pattern of these differences is examined next for several years of operation.

Table 9. Comparison between five neural networks in terms of performance metrics during spring of 2015.

	Network	RMSE	MBE	MAPE	MAE	n RMSE
		W	W	%	W	
10 April 2015	FFANN	117	49	2.26	102	0.0011
	DFFNN	97	1	2.28	81	0.0009
	RNN	89	4	2.46	78	0.0008
	CFN	113	27	2.05	88	0.0010
	NARX	191	113	3.42	161	0.0018
11 April 2015	FFANN	152	109	2.90	130	0.0014
	DFFNN	140	93	2.54	120	0.0013
	RNN	153	113	2.86	130	0.0014
	CFN	153	107	3.08	130	0.0014
	NARX	149	109	3.21	129	0.0013
12 April 2015	FFANN	127	102	2.02	111	0.0012
	DFFNN	128	102	2.22	112	0.0012
	RNN	128	103	2.30	113	0.0012
	CFN	126	97	2.70	109	0.0012
	NARX	123	101	2.44	108	0.0011
13 April 2015	FFANN	105	71	2.58	96	0.0010
	DFFNN	103	73	1.90	89	0.0010
	RNN	114	82	2.33	100	0.0011
	CFN	114	80	2.75	103	0.0011
	NARX	119	94	2.60	103	0.0011

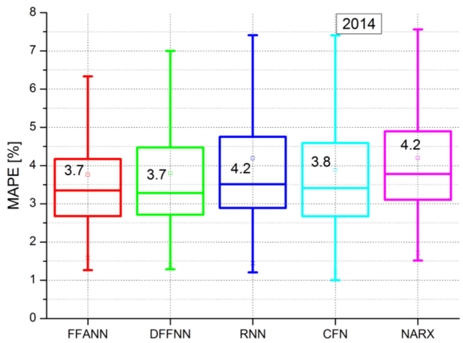

Figure 15. Comparison of five networks during 2014 in terms of MAPE.

Figure 16 follows, in general, the same pattern as far as differences between networks is concerned. The DFFNN and FFANN have lower errors than the other networks, and median values are reported to be around 4.3%. The MAPE of RNN is reported to be of a higher value during 2015, especially the median values of around 4.9%, with the next higher values reported for NARX with median values of around 4.8%. The CF ANN shows slightly higher values than the DFFNN and FFANN with median values around 4.5%. Figure 16 shows that the MAPE values for 2015 year are reported to be between 4.3 and 4.8%, depending on the type of neural network. Comparing Figure 15 with Figure 16, slightly lower MAPE values can be observed, ranging from 3.7–4.2% to 4.3–4.8%. Comparing the evolution of the performance of each network between 2014 and 2015, an increasing trend in all networks is observed.

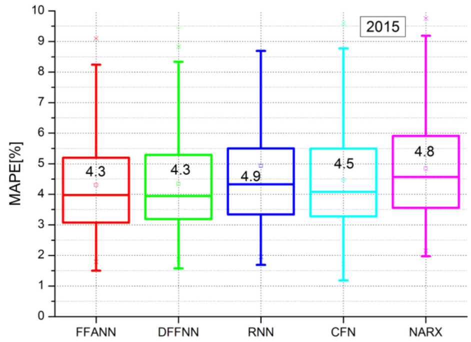

Figure 16. Comparison of five networks during 2015 in terms of MAPE.

Figure 17 generally follows the same pattern as far as differences between the networks are concerned. The DFFNN and FFANN are lower in terms of error values than the other networks, and median values are reported to be around 5.1%. The MAPE of the RNN is reported to be of a higher value during 2016, especially the median values of around 5.6%, with the next higher values reported for NARX with median values of around 5.6%. The CFN shows slightly higher values than the DFFNN and FFANN with median values of around 5.3%. Figure 17 shows that the MAPE values for the 2016 year are reported to be between 5.1 and 5.6%, depending on the type of neural network. Comparing Figure 17 with Figure 15, however, the MAPE is about 1.5 units higher compared to 2014 for all networks from 3.7–4.2% to 5.1–5.6% in terms of median values.

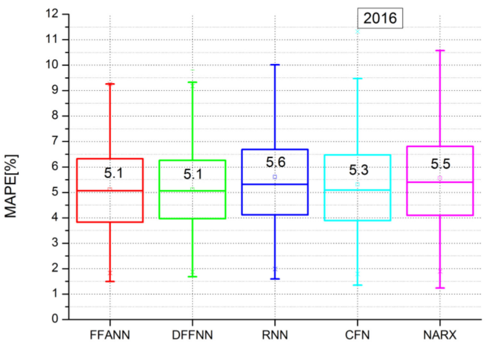

Figure 17. Comparison of five networks during 2016 in terms of MAPE.

The same pattern between networks behavior is also observed in Figure 18. The DFFNN with median values of MAPE at 4.2% and the FFANN with median values of MAPE at 4.4% are lower in terms of error than the other networks. The MAPE of NARX is reported to be of a higher value during 2017, especially the median values of around 4.8%, with the next higher values reported for the RNN with median values of around 4.6%. The CFN shows slightly higher values than DFFNN and FFANN with median values of around 4.5%. Figure 18 shows that the MAPE values for the 2017 year are reported to be between 4.2 and 4.8%, depending on the type of neural network. However, the time values are lower compared to 2016, higher compared to 2014, and at the same level as 2015.

Figure 19 presents results from 2018. The DFFNN with median values of MAPE at 5.4% and the FFANN with median values of MAPE at 5.5% are lower in terms of error than the other networks. The MAPE of the RNN is reported to be of a higher value during 2018, especially the median values of around 5.8%, with the next higher values reported for NARX with median values of around 5.7%. The CFN shows slightly higher values than the DFFNN and FFANN with median values of around 5.6%. Figure 19 shows that the MAPE values for the 2018 year are reported to be between 5.4 and 5.8%, depending on the type of neural network.

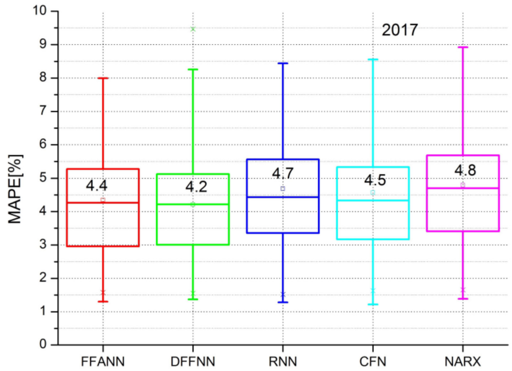

Figure 18. Comparison of the five networks' performance during 2017 in terms of MAPE.

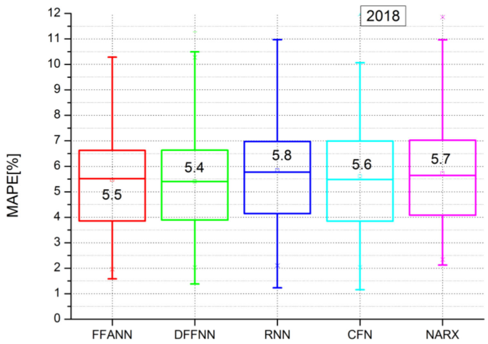

Figure 19. Comparison of the five networks' performance during 2018 in terms of MAPE.

Figure 20 presents results from 2019. The DFFNN and FFANN with median values of MAPE at 6.2% are lower in terms of error than the other networks. The MAPE of the RNN and NARX is reported to higher in value during 2019, especially median values of around 6.6%, with the next higher values reported for the CFN that shows median values of around 6.5%. Figure 19 shows that the MAPE values for the 2019 year are reported to be between 6.2 and 6.6%, depending on the type of neural network.

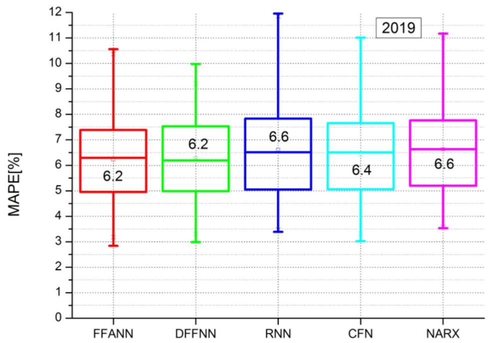

Figure 20. Comparison of the five networks' performance during 2019 in terms of MAPE.

Figure 21 presents results from 2020. The DFFNN and CFN with median values of MAPE at 5.3% and the RNN with median values of MAPE at 5.5% are lower in terms of error than the other networks. The MAPE of NARX is reported to be of higher value during 2020, especially median values of around 5.9%, with the next higher values reported for FFANN that shows median values at around 5.7%. Figure 20 shows that the MAPE values for the 2020 year are reported to be between 5.3 and 5.9%, depending on the type of neural network.

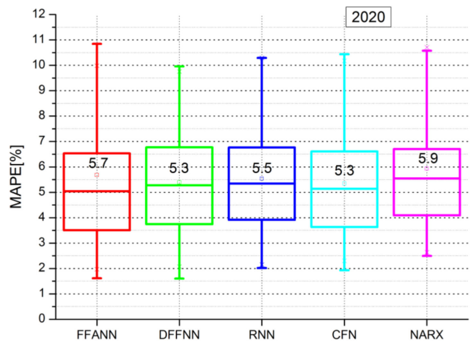

Figure 21. Comparison of the five networks' performance during 2020 in terms of MAPE.

Figures 19–21 present the annual periods of 2018 to 2020, respectively. The reported values of MAPE are significantly higher for all networks compared to the period of 2014–2017. It is clear that the reported value of the MAPE for 2019 (Figure 20) is higher, exceeding 6%. The median values of MAPE from the analysis above are summarized in Table 10.

Table 10. Median values from box charts from Figures 15–21.

Year	Figure	FFANN	DFFNN	RNN	CFN	NARX
2014	Figure 15	3.7	3.7	4.2	3.8	4.2
2015	Figure 16	4.3	4.3	4.9	4.5	4.8
2016	Figure 17	5.1	5.1	5.6	5.3	5.5
2017	Figure 18	4.4	4.2	4.7	4.5	4.8
2018	Figure 19	5.5	5.4	5.8	5.6	5.7
2019	Figure 20	6.2	6.2	6.6	6.4	6.6
2020	Figure 21	5.7	5.3	5.5	5.3	5.9

From the above-mentioned analysis, it is concluded that the DFFNN achieves overall better performance because the reported values of MAPE are the lowest among all types of networks. According to this fact, the DFFNN is selected to act as the baseline among the proposed NNs in the comparative analysis, which is presented below. In order to investigate the long-term performance of PV systems, the performance metrics of the DFFNN are selected to be used as indicators of faults compared with mean normalized efficiency, which was calculated in Section 2. Figure 22 shows the evolution of the MAPE in the period of 2014 to 2020, where a nonlinearly increasing trend is observed. Days with reported faults are rejected from Figure 22 in order to decouple the effect of degradation. The error in these faulty conditions was over 30% for faults in a string, whereas a faulty panel was associated with a deviation of 10–20% and faults of near shading of 6–10% compared to 5% during normal operation [58]. Most of the PV panels' manufacturers declare a linear degradation of the semiconductor, which is included in the warranty conditions. In this case study, a decreasing trend is indeed observed; however, this is not linear, which could be explained by the dust accumulation and cleaning effect. Dust effects have a significant impact on PV performance, particularly resulting in a decrease of 5.6% on heavily soiled panels [59] in Central Greece and a 5% power output reduction, even after a small period of time PV exposure into the atmospheric air pollution in Athens [60]. In southern regions, PV modules are reported to decrease in their produced power by 12%, 6%, 6%, 7%, 3%, 4%, and 4%, for ash, calcium carbonate, limestone, cement, sulfur, sawdust, and brown soil, respectively [61].

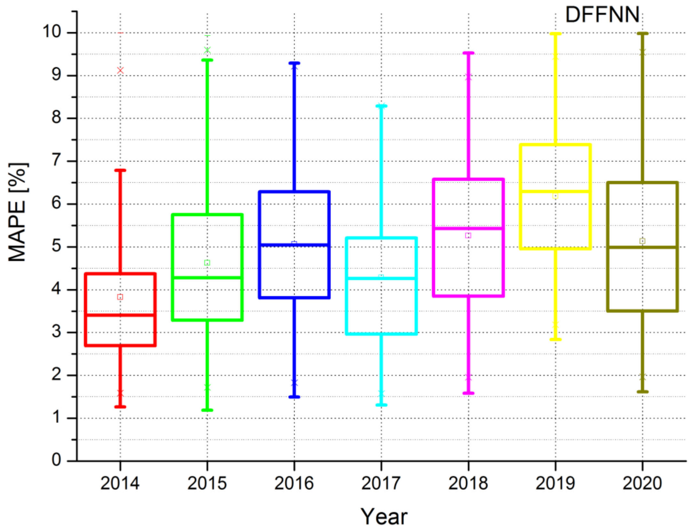

Figure 22. Evolution of DFNN prediction MAPE during several years of operation.

The increasing trend in MAPE in Figure 22 is correlated with the decreasing trend in normalized efficiency in Figure 23 during 2013–2014. This holds especially for air mass values 1–3. Both approaches converge to the finding that performance during the year 2019 is significantly lower than that of 2014. However, actual electricity generation was lower during 2014 (Table 1) because of the reported faults and weather conditions. The fact that efficiency is higher in 2020 compared to 2019 could possibly be due to increased dust accumulation during 2019.

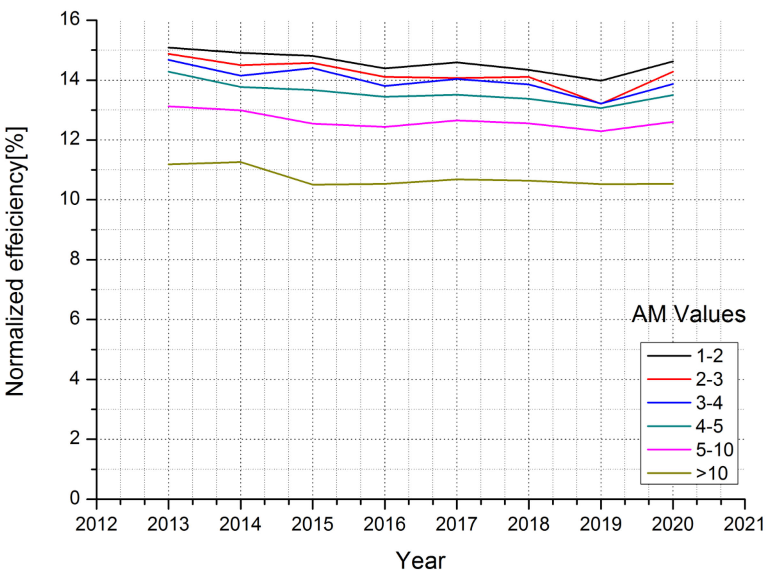

Figure 23. Evolution of DFNN predictions MAPE during several years of operation.

Combining results from Figures 22 and 23, we conclude that the PV system's performance shows a decreasing trend, which is influenced by stochastic dust accumulation and cleaning effects. Using the performance metrics of NN application predictions, this method estimates a decreasing trend in performance. However, this method is not proposed for future predictions based on data from just the first year of operation. Another important conclusion is that electricity production forecasting should take into account, as additional input, the degradation rate of PV panels.

4. Conclusions

This paper studies the performance of a grid-connected PV system in Central Greece. Energy generation per installed DC power fluctuated between 1437.1 to 1611.5 kWh/kWp. The maximum generation was observed during the first year of operation. The application of five different ANNs, namely (i) feed-Forward network (one hidden layer), (ii) deep feed-forward network (two hidden layers), (iii) recurrent neural network, (iv) cascade-forward network, and (v) nonlinear autoregressive network, was employed with the following five inputs: in- plane irradiance, backsheet panel temperature, air mass, clearness index, and DC voltage of the inverter. The DFFNN (3.7 to 6.2 %) and FFANN (3.7 to 6.2%) have slightly better performance compared to CFN (3.8 to 6.6%). On the other hand, NARX (4.2 to 6.6%) and RNN (4.2 to 6.6%) have higher values MAPE every year. MAPE values show an increasing trend over the years. This fact indicates a possible change in PV performance. It also suggests that long-term energy forecasting should embed data from a whole year period for accurate prediction. The DFFNN prediction is used as a baseline and compared to actual data. The performance metrics of DFFNN application act as indicators, in combination with normalized efficiency, and point to a performance decrease trend, which is also influenced by dust accumulation and cleaning effects. However, this method is not proposed for future predictions based on data from just the first year of operation. Another important conclusion is that electricity forecasting should take into account, as an additional input, the degradation rate of PV panels. The proposed methodology is appropriate for PV performance evaluation using real data from grid-connected PV systems when networks are trained with data from the first year of operation. A possible task for future work is to train neural networks with data from several years of operation in order to accurately predict future energy generation.

Author Contributions: Conceptualization, E.R. and T.S.; methodology, E.R.; software, E.R. and T.S.; validation, E.R.; formal analysis, E.R.; investigation, E.R.; writing—original draft preparation, E.R.; writing—review and editing, T.S. All authors have read and agreed to the published version of the manuscript.

Funding: This research received no external funding.

Institutional Review Board Statement: Not applicable.

Informed Consent Statement: Not applicable.

Data Availability Statement: Not applicable.

Conflicts of Interest: The authors declare no conflict of interest.

Abbreviations

PV	Photovoltaic
RES	Renewable Energy Sources
IRENA	International Renewable Energy Agency
ANN	Artificial Neural Networks
HVAC	Heating Ventilation Air Conditioning
CHP	Combined Heat and Power
EV	Electric Vehicles
HFCV	Hydrogen Fuel-Cell Vehicles
MLP	Multi-Layer Perceptron
DNN	Deep Neural Network
LSTM	Long Short-Term Memory
CNN	Convolutional Neural Networks
ANFIS	Adaptive Neuro-Fuzzy Inference System
RSM	Response Surface Methodology
AI	Artificial intelligence

SA	Simple Average
SMA	Simple Moving Average
NAR	Nonlinear Autoregressive
SVM	Support Vector Machine (SVM)
GPR	Gaussian process regression
NN	Neural Networks
MAE	Mean Absolute Error
RMSE	Root Mean Square Error
MAPE	Mean Absolute Percentage Error
PR	Performance Ratio
RNN	Recurrent Neural Network
BD-LSTM	Bi-directional Long Short-Term Memory
EMA	Exponential Moving Average
PV-T	Photovoltaic Thermal
R^2	Correlations Coefficient
MLF	Multi-layer Feed Forward
API	Applications Programming Interface
IR	Infrared
NARX	Nonlinear Autoregressive Exogenous
MPPT	Maximum Power Point Tracking
CUF	Capacity Utilization Factor
STL	Scatterplot Smoothing
AM	Airmass
MBE	Mean Bias Error
Kt	Daily Clearness Index

Appendix A

Table A1. Technical Characteristics of PV panels.

Yingli 60 Cell YGE SERIES			
Module Type		**YL240P-29b**	
		STC	NOCT
Power output	W	240	174.3
Module efficiency	%	14.7	13.3
Voltage at P_{max}	W	29.5	26.6
Current at P_{max}	A	8.14	6.56
Open-circuit voltage	V	37.5	34.2
Short-circuit current	A	8.65	7.01
Normal operating cell temperature (NOCT)	°C	46+/−2	
Temperature coefficient of P_{max}	%/°C	−0.45	
Temperature coefficient of V_{oc}	%/°C	−0.33	
Temperature coefficient of I_{sc}	%/°C	0.06	
Temperature coefficient of V_{mpp}	%/°C	−0.45	
Dimensions(L/W/H)	mm	1650/990/40	
STC: 1000 W/m^2 irradiance, 25 °C cell temperature, AM1.5 G spectrum according to EN 60904-3			
Average relative efficiency reduction of 5% at 200 W/m^2 according to EN 60904-3			
NOCT: open-circuit module operation temperature at 800 W/m^2 irradiance, 20 °C ambient temperature, 1 m/s wind speed			

Table A2. Technical characteristics and efficiency ratings.

Fronius IG Plus 150V-3		
$P_{DC,MAX}$	W	12,770
$I_{DC,MAX}$	A	55.5
$U_{DC,MIN}$	V	230
$U_{DC,START}$	V	260
$U_{DC,R}$	V	370
$U_{DC,MAX}$	V	600
$P_{AC,R}$	W	12,000
$I_{AC,MAX}$	A	17.4
$U_{AC,R}$	V	3-NPE 400/230
Maximum efficiency n_{inv}	%	95.9
n_{inv} at 5% $P_{AC,R}$ (230 V/370 V/500 V)	%	91.8/92.5/91.1
n_{inv} at 10% $P_{AC,R}$ (230 V/370 V/500 V)	%	91.0/94.3/93.2
n_{inv} at 20% $P_{AC,R}$ (230 V/370 V/500 V)	%	94.7/95.1/94.6
n_{inv} at 25% $P_{AC,R}$ (230 V/370 V/500 V)	%	95.1/95.3/94.7
n_{inv} at 30% $P_{AC,R}$ (230 V/370 V/500 V)	%	95.1/95.3/94.9
n_{inv} at 50% $P_{AC,R}$ (230 V/370 V/500 V)	%	95.3/95.9/95.3
n_{inv} at 75% $P_{AC,R}$ (230 V/370 V/500 V)	%	94.7/95.6/95.4
n_{inv} at 100% $P_{AC,R}$ (230 V/370 V/500 V)	%	94.0/95.2/95.1
$P_{DC,MAX}$	W	12,770
$I_{DC,MAX}$	A	55.5
$U_{DC,MIN}$	V	230
$U_{DC,START}$	V	260

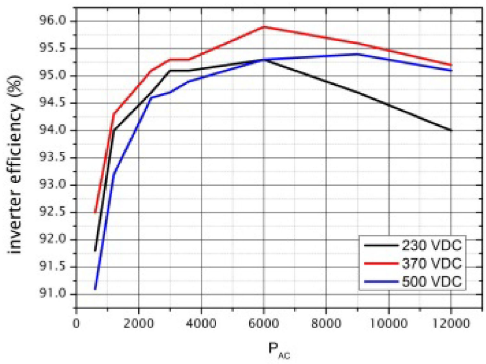

Figure A1. Efficiency curve of inverter with the AC power for different DC voltages.

Table A3. Irradiance sensor characteristics.

Sensor	**Mono-Crystalline Si-Sensor**
Sensor voltage	75 mV at 1000 W/m^2 (exact calibration voltage written on sensor)
Accuracy	±5% (average of a year)
Ambient temperature	−40 °C to +85 °C
Design	Sensor mounted on z-shaped aluminum profile
Dimensions	L × W × H = 55 × 55 × 10 mm
Fronius Product Nr.	43,0001,1189

Table A4. Temperature sensor characteristics.

Sensor	**PT 100**
Measuring Range	−40 °C to +188 °C
Accuracy	±0.8 °C (in the range −40 °C to +100 °C)
Design	Sensor on an adhesive film for measurements on surfaces
Dimensions	32 × 32 mm
Fronius Art.Nr.	43,0001,1190

Appendix B

Definition of important performance metrics

$$Y_F = \frac{E}{P_{STC}}\left(\frac{kWh}{kW}\right)$$

$$Y_R = \frac{H}{G_{STC}}\left(\frac{kWh}{kW}\right)$$

$$PR = \frac{Y_F}{Y_R}$$

References

1. IRENA. *Renewable Capacity Highlights*; IRENA: Masdar City, United Arab Emirates, 2022.
2. DAPEEP. Operator of RES and Guarantees of Origin (DAPEEP S.A.). 2023. Available online: https://www.dapeep.gr/ (accessed on 6 May 2023).
3. Stamatellou, A.-M.; Zogou, O.; Stamatelos, A. Energy Cost Assessment and Optimization of Post-COVID-19 Building Ventilation Strategies. *Sustainability* **2023**, *15*, 3422. [CrossRef]
4. Noro, M.; Mancin, S.; Busato, F.; Cerboni, F. Innovative Hybrid Condensing Radiant System for Industrial Heating: An Energy and Economic Analysis. *Sustainability* **2023**, *15*, 3037. [CrossRef]
5. Stamatellos, G.; Zogou, O.; Stamatelos, A. Energy Performance Optimization of a House with Grid-Connected Rooftop PV Installation and Air Source Heat Pump. *Energies* **2021**, *14*, 740. [CrossRef]
6. Stamatellos, G.; Zogou, O.; Stamatelos, A. Energy Analysis of a NZEB Office Building with Rooftop PV Installation: Exploitation of the Employees’ Electric Vehicles Battery Storage. *Energies* **2022**, *15*, 6206.
7. Göhler, G.; Klingler, A.-L.; Klausmann, F.; Spath, D. Integrated Modelling of Decentralised Energy Supply in Combination with Electric Vehicle Charging in a Real-Life Case Study. *Energies* **2021**, *14*, 6874. [CrossRef]
8. Pai, L.; Senjyu, T. A Yearly Based Multiobjective Park-and-Ride Control Approach Simulation Using Photovoltaic and Battery Energy Storage Systems: Fuxin, China Case Study. *Sustainability* **2022**, *14*, 8655. [CrossRef]
9. Kelepouris, N.; Nousdilis, A.; Bouhouras, A.; Christoforidis, G. Optimal scheduling of prosumer's battery storage and flexible loads for distribution network support. *IET Gener. Transm. Distrib.* **2023**, *17*, 1491–1508. [CrossRef]
10. Vodapally, S.N.; Ali, M.H. A Comprehensive Review of Solar Photovoltaic (PV) Technologies, Architecture, and Its Applications to Improved Efficiency. *Energies* **2023**, *16*, 319. [CrossRef]
11. Jamil, U.; Bonnington, A.; Pearce, J.M. The Agrivoltaic Potential of Canada. *Sustainability* **2023**, *15*, 3228. [CrossRef]
12. Huang, X.; Qu, Y.; Zhu, Z.; Wu, Q. Techno-Economic Analysis of Photovoltaic Hydrogen Production Considering Technological Progress Uncertainty. *Sustainability* **2023**, *15*, 3580. [CrossRef]
13. Gulzar, M.M. Maximum Power Point Tracking of a Grid Connected PV Based Fuel Cell System Using Optimal Control Technique. *Sustainability* **2023**, *15*, 3980. [CrossRef]
14. Zhu, L.; He, J.; He, L.; Huang, W.; Wang, Y.; Liu, Z. Optimal Operation Strategy of PV-Charging-Hydrogenation Composite Energy Station Considering Demand Response. *Energies* **2022**, *15*, 5915. [CrossRef]
15. Gulkowski, S.; Zdyb, A.; Dragan, P. Experimental Efficiency Analysis of a Photovoltaic System with Different Module Technologies under Temperate Climate Conditions. *Appl. Sci.* **2019**, *9*, 141. [CrossRef]
16. Li, B.; Delpha, C.; Diallo, D.; Migan-Dubois, A. Application of Artificial Neural Networks to photovoltaic fault detection and diagnosis: A review. *Renew. Sustain. Energy Rev.* **2021**, *138*, 110512. [CrossRef]
17. Kontogiannis, D.; Bargiotas, D.; Daskalopulu, A.; Arvanitidis, A.I.; Tsoukalas, L.H. Error Compensation Enhanced Day-Ahead Electricity Price Forecasting. *Energies* **2022**, *15*, 1466. [CrossRef]
18. López Gómez, J.; Ogando Martínez, A.; Troncoso Pastoriza, F.; Febrero Garrido, L.; Granada Álvarez, E.; Orosa García, J.A. Photovoltaic Power Prediction Using Artificial Neural Networks and Numerical Weather Data. *Sustainability* **2020**, *12*, 10295. [CrossRef]
19. Gopi, A.; Sharma, P.; Sudhakar, K.; Ngui, W.K.; Kirpichnikova, I.; Cuce, E. Weather Impact on Solar Farm Performance: A Comparative Analysis of Machine Learning Techniques. *Sustainability* **2023**, *15*, 439. [CrossRef]
20. Kolsi, L.; Al-Dahidi, S.; Kamel, S.; Aich, W.; Boubaker, S.; Ben Khedher, N. Prediction of Solar Energy Yield Based on Artificial Intelligence Techniques for the Ha’il Region, Saudi Arabia. *Sustainability* **2023**, *15*, 774.
21. Lim, S.-C.; Huh, J.-H.; Hong, S.-H.; Park, C.-Y.; Kim, J.-C. Solar Power Forecasting Using CNN-LSTM Hybrid Model. *Energies* **2022**, *15*, 8233. [CrossRef]
22. Suresh, V.; Janik, P.; Rezmer, J.; Leonowicz, Z. Forecasting Solar PV Output Using Convolutional Neural Networks with a Sliding Window Algorithm. *Energies* **2020**, *13*, 723. [CrossRef]

23. Andrade, C.H.T.d.; Melo, G.C.G.d.; Vieira, T.F.; Araújo, Í.B.Q.d.; Medeiros Martins, A.d.; Torres, I.C.; Brito, D.B.; Santos, A.K.X. How Does Neural Network Model Capacity Affect Photovoltaic Power Prediction? A Study Case. *Sensors* **2023**, *23*, 1357. [CrossRef] [PubMed]
24. Kim, Y.; Seo, K.; Harrington, R.J.; Lee, Y.; Kim, H.; Kim, S. High Accuracy Modeling for Solar PV Power Generation Using Noble BD-LSTM-Based Neural Networks with EMA. *Appl. Sci.* **2020**, *10*, 7339. [CrossRef]
25. Preda, S.; Oprea, S.-V.; Bâra, A.; Belciu, A. PV Forecasting Using Support Vector Machine Learning in a Big Data Analytics Context. *Symmetry* **2018**, *10*, 748. [CrossRef]
26. Metlek, S.; Kandilli, C.; Kayaalp, K. Prediction of the effect of temperature on electric power in photovoltaic thermal systems based on natural zeolite plates. *Int. J. Energy Res.* **2021**, *46*, 6370–6382. [CrossRef]
27. Yuan, Z.; Xiong, G.; Fu, X. Artificial Neural Network for Fault Diagnosis of Solar Photovoltaic Systems: A Survey. *Energies* **2022**, *15*, 8693. [CrossRef]
28. Samara, S.; Natsheh, E. Intelligent PV Panels Fault Diagnosis Method Based on NARX Network and Linguistic Fuzzy Rule-Based Systems. *Sustainability* **2020**, *12*, 2011. [CrossRef]
29. Onim, M.S.H.; Sakif, Z.M.M.; Ahnaf, A.; Kabir, A.; Azad, A.K.; Oo, A.M.T.; Afreen, R.; Hridy, S.T.; Hossain, M.; Jabid, T.; et al. SolNet: A Convolutional Neural Network for Detecting Dust on Solar Panels. *Energies* **2023**, *16*, 155. [CrossRef]
30. Selvaraj, T.; Rengaraj, R.; Venkatakrishnan, G.; Soundararajan, S.; Natarajan, K.; Balachandran, P.; David, P.; Selvarajan, S. Environmental Fault Diagnosis of Solar Panels Using Solar Thermal Images in Multiple Convolutional Neural Networks. *Int. Trans. Electr. Energy Syst.* **2022**, *2022*, 2872925. [CrossRef]
31. Lu, X.; Lin, P.; Cheng, S.; Fang, G.; He, X.; Chen, Z.; Wu, L. Fault diagnosis model for photovoltaic array using a dual-channels convolutional neural network with a feature selection structure. *Energy Convers. Manag.* **2021**, *248*, 114777. [CrossRef]
32. Yu, W.; Liu, G.; Zhu, L.; Yu, W. Convolutional neural network with feature reconstruction for monitoring mismatched photovoltaic systems. *Sol. Energy* **2020**, *212*, 169–177. [CrossRef]
33. Yousif, J.H.; Kazem, H.A.; Al-Balushi, H.; Abuhmaidan, K.; Al-Badi, R. Artificial Neural Network Modelling and Experimental Evaluation of Dust and Thermal Energy Impact on Monocrystalline and Polycrystalline Photovoltaic Modules. *Energies* **2022**, *15*, 4138. [CrossRef]
34. Tripathi, A.K.; Aruna, M.; Venkatesan, E.P.; Abbas, M.; Afzal, A.; Shaik, S.; Linul, E. Quantitative Analysis of Solar Photovoltaic Panel Performance with Size-Varied Dust Pollutants Deposition Using Different Machine Learning Approaches. *Molecules* **2022**, *27*, 7853. [CrossRef]
35. Iqbal, M.S.; Niazi, Y.A.K.; Amir Khan, U.; Lee, B.-W. Real-time fault detection system for large scale grid integrated solar photovoltaic power plants. *Int. J. Electr. Power Energy Syst.* **2021**, *130*, 106902. [CrossRef]
36. Minai, A.F.; Usmani, T.; Alotaibi, M.A.; Malik, H.; Nassar, M.E. Performance Analysis and Comparative Study of a 467.2 kWp Grid-Interactive SPV System: A Case Study. *Energies* **2022**, *15*, 1107. [CrossRef]
37. Karahüseyin, T.; Abbasoğlu, S. Performance Loss Rates of a 1 MWp PV Plant with Various Tilt Angle, Orientation and Installed Environment in the Capital of Cyprus. *Sustainability* **2022**, *14*, 9084. [CrossRef]
38. Agyekum, E.B.; Mehmood, U.; Kamel, S.; Shouran, M.; Elgamli, E.; Adebayo, T.S. Technical Performance Prediction and Employment Potential of Solar PV Systems in Cold Countries. *Sustainability* **2022**, *14*, 3546. [CrossRef]
39. Shin, J.-H.; Kim, J.-O. On-Line Diagnosis and Fault State Classification Method of Photovoltaic Plant. *Energies* **2020**, *13*, 4584. [CrossRef]
40. Phuong Truong, L.; An Quoc, H.; Tsai, H.-L.; Van Dung, D. A Method to Estimate and Analyze the Performance of a Grid-Connected Photovoltaic Power Plant. *Energies* **2020**, *13*, 2583. [CrossRef]
41. Dhimish, M. Performance Ratio and Degradation Rate Analysis of 10-Year Field Exposed Residential Photovoltaic Installations in the UK and Ireland. *Clean Technol.* **2020**, *2*, 170–183. [CrossRef]
42. Bansal, N.; Jaiswal, S.P.; Singh, G. Long term operational performance and experimental on-field degradation measurement of 10 MW PV plant in remote location in India. *Energy Sustain. Dev.* **2022**, *67*, 135–150. [CrossRef]
43. Trillo-Montero, D.; Cosano-Lucena, S.; Gonzalez-Redondo, M.; Luna-Rodriguez, J.J.; Santiago, I. Design and Development of a Relational Database Management System (RDBMS) with Open Source Tools for the Processing of Data Monitored in a Set of Photovoltaic (PV) Plants. *Appl. Sci.* **2023**, *13*, 1357. [CrossRef]
44. Son, N.; Jung, M. Analysis of Meteorological Factor Multivariate Models for Medium- and Long-Term Photovoltaic Solar Power Forecasting Using Long Short-Term Memory. *Appl. Sci.* **2021**, *11*, 316. [CrossRef]
45. Sun, Y.; Wang, F.; Wang, B.; Chen, Q.; Engerer, N.A.; Mi, Z. Correlation Feature Selection and Mutual Information Theory Based Quantitative Research on Meteorological Impact Factors of Module Temperature for Solar Photovoltaic Systems. *Energies* **2017**, *10*, 7. [CrossRef]
46. Konstantinou, M.; Peratikou, S.; Charalambides, A.G. Solar Photovoltaic Forecasting of Power Output Using LSTM Networks. *Atmosphere* **2021**, *12*, 124. [CrossRef]
47. Das, U.; Tey, K.S.; Idris, M.; Mekhilef, S.; Seyedmahmoudian, M.; Horan, B.; Stojcevski, A. Forecasting of Photovoltaic Power Generation and Model Optimization. *Renew. Sustain. Energy Rev.* **2017**, *81*, 912–928. [CrossRef]
48. Bergmann, A. (Ed.) *Photovoltaikanlagen*; VDE VERLAG Berlin: Offenbach, Germany, 2011.
49. Roumpakias, E.; Stamatelos, A. Comparative performance analysis of grid-connected photovoltaic system by use of existing performance models. *Energy Convers. Manag.* **2017**, *150*, 14–25. [CrossRef]

50. Tawa, H.; Saiki, H.; Ota, Y.; Araki, K.; Takamoto, T.; Nishioka, K. Accurate Output Forecasting Method for Various Photovoltaic Modules Considering Incident Angle and Spectral Change Owing to Atmospheric Parameters and Cloud Conditions. *Appl. Sci.* **2020**, *10*, 703. [CrossRef]
51. Poczeta, K.; Papageorgiou, E.I. Energy Use Forecasting with the Use of a Nested Structure Based on Fuzzy Cognitive Maps and Artificial Neural Networks. *Energies* **2022**, *15*, 7542. [CrossRef]
52. Starzyński, J.; Zawadzki, P.; Harańczyk, D. Machine Learning in Solar Plants Inspection Automation. *Energies* **2022**, *15*, 5966. [CrossRef]
53. Hagan, M.T.; Demuth, H.B.; Beale, M.H.; DeJesus, O. Neural Network Design; Martin Hagan. 2014. Available online: https://hagan.okstate.edu/NNDesign.pdf (accessed on 6 May 2023).
54. Aslam, M.; Lee, J.-M.; Kim, H.-S.; Lee, S.-J.; Hong, S. Deep Learning Models for Long-Term Solar Radiation Forecasting Considering Microgrid Installation: A Comparative Study. *Energies* **2020**, *13*, 147. [CrossRef]
55. Nawab, F.; Abd Hamid, A.S.; Alwaeli, A.; Arif, M.; Fauzan, M.F.; Ibrahim, A. Evaluation of Artificial Neural Networks with Satellite Data Inputs for Daily, Monthly, and Yearly Solar Irradiation Prediction for Pakistan. *Sustainability* **2022**, *14*, 7945. [CrossRef]
56. Boussaada, Z.; Curea, O.; Remaci, A.; Camblong, H.; Mrabet Bellaaj, N. A Nonlinear Autoregressive Exogenous (NARX) Neural Network Model for the Prediction of the Daily Direct Solar Radiation. *Energies* **2018**, *11*, 620. [CrossRef]
57. Turcu, F.; Lazar, A.; Rednic, V.; Rosca, G.; Zamfirescu, C.; Puschita, E. Prediction of Electric Power Production and Consumption for the CETATEA Building Using Neural Networks. *Sensors* **2022**, *22*, 6259. [CrossRef]
58. Roumpakias, E.; Stamatelos, T. Health Monitoring and Fault Detection in Photovoltaic Systems in Central Greece Using Artificial Neural Networks. *Appl. Sci.* **2022**, *12*, 12016. [CrossRef]
59. Roumpakias, E.; Stamatelos, T. Surface Dust and Aerosol Effects on the Performance of Grid-Connected Photovoltaic Systems. *Sustainability* **2020**, *12*, 569. [CrossRef]
60. Kaldellis, J.; Kokala, A.; Kapsali, M. Natural air pollution deposition impact on the efficiency of PV panels in urban environment. *Fresenius Environ. Bull.* **2010**, *19*, 2864–2872.
61. Kazem, H.A.; Chaichan, M.T.; Al-Waeli, A.H.A.; Sopian, K. Effect of dust and cleaning methods on mono and polycrystalline solar photovoltaic performance: An indoor experimental study. *Sol. Energy* **2022**, *236*, 626–643. [CrossRef]